JOURNAL OF THERMOPHYSICS AND HEAT TRANSFER
Vol. 31, No. 3, July–September 2017

Aerothermochemical Nonequilibrium Modeling for Oxygen Flows

Kevin Neitzel,* Daniil Andrienko,† and Iain D. Boyd‡
University of Michigan, Ann Arbor, Michigan 48109

DOI: 10.2514/1.T4962

The results from a set of vibrational nonequilibrium models with a range of fidelity are compared to the recent experimental data for several postnormal shock test cases. The present work focuses solely on oxygen flows with an emphasis on implementing a new set of accurate state-specific rate coefficients for O_2–O collisions. The two-temperature model is presented as the computationally efficient, lower-fidelity approach in this work. The two-temperature model is driven by the relaxation parameters based on the Millikan–White empirical equation as well as on the parameters resulting from a master equation simulation that employs the database of state-resolved O_2–O rate coefficients. The full state-to-state master equation approach is presented as the higher-fidelity modeling approach. The O_2–O system uses recently available results of trajectory simulations for state-specific transition rate coefficients The O_2–O_2 system uses transition rates from the forced harmonic oscillator model. The test case comparison shows that the state-resolved modeling approach is more suitable for describing the vibrational temperature and chemically nonequilibrium zone behind the shock wave. It is shown that the capability of the state-resolved model to capture non-Boltzmann distribution is critical for accurately modeling the vibrational relaxation and dissociation phase.

Nomenclature

A, B	=	Millikan–White coefficients
C_{VD}	=	vibrational-dissociation factor
E_v	=	vibrational energy, J
E_v^*	=	equilibrium vibrational energy, J
K	=	reaction rate, cm^3/s
P	=	pressure, atm
T_t	=	translational temperature, K
T_v	=	vibrational temperature, K
v	=	vibrational quantum state
μ	=	reduced mass, kg
ρ	=	density, kg/m^3
σ_v	=	collisional cross-section, m^2
τ_v	=	vibrational relaxation time, s

I. Introduction

COMPUTER simulation is the primary analysis tool for hypersonic vehicles. The accuracy of the physics modeling dictates the design margin that is required for the thermal protection system. Many of the hypersonic flight conditions and geometry do not allow the flow to reach equilibrium before interacting with the vehicle. Modeling this nonequilibrium thermochemistry is one of the main sources of simulation uncertainty. Recent advances in computational chemistry methods have made it possible to investigate the use of high-fidelity modeling for hypersonic vehicle analysis.

The two-temperature model is the widely used approach for hypersonic vehicle analysis [1]. For vibrational relaxation, the approach relies on a relaxation time that is a function of temperature and pressure to solve the Landau–Teller equation for vibrational energy. The Millikan–White (MW) formula for vibrational relaxation time is generally used and correlates well with experimental data for many molecular systems [2]. One of the exceptions is the O_2–O system that does not correlate well with experimental data [3,4]. The O_2–O system violates many of the assumptions that are present in the underlying Landau–Teller theory that dictates the temperature dependence of the Millikan–White formula. Park and others have adjusted the Millikan–White coefficients for O_2–O to correlate better with experimental data [5]. However, the previous work has still assumed the temperature dependence dictated by the Landau–Teller theory. The vibrational relaxation of O_2–O is studied in this work using recently developed rates from a detailed quasi-classical trajectory (QCT) analysis [6]. The vibrational relaxation times obtained using the extensive quasi-classical trajectory analysis coupled to the set of master equations indicate that relaxation is the most effective at low temperatures, which is opposite to the temperature dependence assumed in the MW equation. Chemistry is captured by reaction rates that use Arrhenius-type rate coefficients. Additionally, the Arrhenius form uses the geometrically averaged temperature of the translational and vibrational temperature ($T_a = \sqrt{T_t T_v}$) in order to capture nonequilibrium, thermochemical coupling.

The state-to-state (STS) approach is a higher-fidelity model for describing the nonequilibrium energy transfer that has been used sparingly for decades but has become more popular recently due to advances in computational power [7–15]. The STS model is computationally expensive since it directly simulates the population of each vibrational state. These populations are governed by the system of master equations that employ state-specific rates obtained by QCT simulations or simpler models [16]. This approach allows for multiquantum transitions and non-Boltzmann distributions to be captured [7,10,17]. There are three widely used methods for deriving the required transition rate coefficients: the Schwartz, Slawsky, and Herzfeld theory based on first-order perturbation; the forced harmonic oscillator (FHO) model of Adamovich et al. [16]; and the QCT analysis [18]. The presented work will focus on the FHO and QCT methods. The FHO model is a semiclassical analytical method that was developed from nonperturbative analytic theory assuming that the interaction of target and projectile particles is governed by a strong repulsive potential. The closed form of the FHO rate coefficients makes it very attractive due to the low computational expense required to generate transition rates. However, the assumptions including the form of the potential energy surface (PES) put a limitation on the systems that are described well by the FHO methodology. The FHO model is not applicable for molecular systems that have open-shell atoms and molecules, particularly for the O_2–O collisions. The QCT method is a more general approach, and the transition rates can be obtained for any PES. The QCT method employs Monte Carlo methods of statistical sampling of kinetic and internal energy of particles to accumulate a large-scale database of transition event probabilities. The QCT method is computationally expensive, but the recent increase in computational power has made it tractable for atom–diatom interactions.

Received 23 March 2016; revision received 26 September 2016; accepted for publication 30 September 2016; published online 31 January 2017.

*Ph.D. Candidate, Department Aerospace Engineering, 1320 Beal Avenue.
†Postdoctoral Research Fellow, Department Aerospace Engineering, 1320 Beal Avenue.
‡Professor, Department of Aerospace Engineering, 1320 Beal Avenue.

Recently, vibrational temperature behind a shock wave was measured by means of absorption spectroscopy [19,20]. In these measurements, the attenuation of intensity in the UV region of the Schumann–Runge bands was interpreted in terms of an absorption coefficient that is a function of translational and vibrational temperatures of a gas mixture. Vibrational temperature profiles were obtained for the range of translational temperatures between 4000 and 10,400 K at the incident shock velocity between 3.07 and 4.44 km/s.

The aim of the present work is the numerical simulation of these experimental data using new information on O_2–O collisions that was obtained by means of a QCT study [6,21]. For this purpose, a simpler two-temperature (2T) model adopts new relaxation parameters and global dissociation rates [21]. This approach is compared to the similar model with the rates previously derived for the $O_2 - O$ interaction without relying on the QCT and master equation simulations [1]. Additionally, the present paper performs a complete state-resolved simulation of shock wave propagation in pure oxygen. This is performed by employing the QCT rate coefficients for O_2–O interaction and the FHO model for O_2–O_2 collisions. The novelty of the present work is in the comparison of newly generated experimental data with the theoretical model incorporating high-fidelity rate coefficients derived from first principles.

II. Thermochemical Nonequilibrium Model

In the present work, the postnormal shock calculations use the jump conditions derived from the Rankine–Hugoniot relations. The derivation assumes that the electronic and vibrational modes are frozen across the shock wave. The flow downstream of the shock wave is calculated by solving the one-dimensional compressible flow equations combined with the conservation equations associated with the vibrational energy mode. The compressible flow equations are shown in Eq. (1),

$$\frac{\partial}{\partial x}\begin{pmatrix} \rho_s u \\ \rho u^2 + p \\ \rho u\left(h + u^2/2\right) \end{pmatrix} = \begin{pmatrix} \omega_s \\ 0 \\ 0 \end{pmatrix} \tag{1}$$

where ρ and ρ_s are the densities of the local flow and of the species s; u, P, and h are the local flow velocity, pressure, and enthalpy; and ω_s is the production rate of species s due to chemical reactions. The system of Euler Eq. (1) is closed by the ideal gas law and enthalpy equation. Enthalpy is defined as $h_s = h_0 + 2.5RT + (e_r + e_v)$ and is multiplied by the molar concentration of the species to close the system.

The conservation equations for vibrational energy are formulated individually for the 2T and STS models and given in the following sections.

A. Two-Temperature Model

In the 2T model, nonequilibrium in the energy transfer is described by separating the transrotational energy $e_t(T)$ and the vibration-electronic energy $e_v(T_v)$. The present work accounts for only the ground electronic state. The conservation equation for vibrational energy has the appearance

$$\frac{\partial(\rho e_v)}{\partial x} = \rho_{O_2}\frac{e_v^\star - e_v}{\tau_v(T_a)} + \dot{\omega}_{O_2} C_{\mathrm{VD}}(T) D_e \tag{2}$$

where $\dot{\omega}_{O_2} = R(T_a)n_O^3 - D(T_a)n_{O_2}n_O$; D and R are the global dissociation and recombination rate coefficients evaluated at some effective temperature T_a, respectively, defined in the following; n is the number density; e_v and $e_v^\star$ are the mean vibrational energy evaluated at translational T and vibrational T_{vib} temperatures, respectively; C_{VD} is the vibration–dissociation coupling coefficient that indicates the average loss of vibrational energy in collision of particles that leads to dissociation; τ_v is the relaxation time of the entire vibrational manifold; and D_e is the classical dissociation energy of diatomic O_2. It should be noted that the experimental comparisons in the presented work are done in the time domain. A transformation from the postshock position domain into the time domain is done using the local velocity and shock velocity.

The present work studies three aspects of the two-temperature modeling: the vibrational–translational energy relaxation, dissociation rate, and vibrational energy loss due to dissociation. The newly available QCT data for the O_2–O system allow for modifications to be made in each of these three areas for the 2T model. The results section will demonstrate the isolated and combined effects of these modifications relative to the 2T model implementation.

1. *Vibrational–Translational Energy Transfer*

The relaxation time τ_v in Eq. (2) can be obtained from various methods. The most widely accepted method is the Millikan–White relaxation time shown in Eq. (3). The values for A and B are unique for each interaction of colliding species and can be calculated based on the reduced mass and vibrational characteristic temperature, $A = 0.00116\,\mu^{1/2}\theta^{4/3}$ and $B = 0.015\,\mu^{1/4}$,

$$P\tau_v = \exp[A(T^{-1/3} - B) - 18.42], \qquad \text{atm-s} \tag{3}$$

The Millikan–White relaxation time is modified with the collision-limited correction term shown in Eqs. (4) and (5). It is also referred to as the high-temperature correction. The correction terms include the number density n and the mean particle velocity c. In this work, σ_v^* is set to 3.0×10^{-21} m^2 as proposed by Park [5],

$$\tau_{\mathrm{Park}} = 1/(n\sigma_v c), \ \text{s} \tag{4}$$

$$\sigma_v = \sigma_v^*(50,000/T)^2, \ \text{m}^2 \tag{5}$$

The present work adopts the Millikan–White relaxation time for the O_2–O_2 system [5,16]. However, the assumptions inherent in this model do not apply well to a system containing a molecule and an open-shell atom, like the O_2–O system [22,23]. These types of systems deviate from these model assumptions due to the effect of additional mechanisms such as nonadiabatic transitions and the possibility of atom exchange. The experimental data for the O_2–O system have been shown to not follow the Millikan–White suggested behavior. Park [5] proposed Millikan–White coefficients for O_2–O based on the data from [4]; however, the temperature dependence was still assumed to be consistent with the MW empirical correlations for τ_v. The widely accepted Millikan–White coefficients for O_2–O are $A = 47.7$ and $B = 0.0271$. For O_2–O_2, the Millikan–White coefficients are $A = 135.91$ and $B = 0.030$.

One of the main areas of focus for this work is to use the newly available QCT calculated transition rates for O_2–O from Andrienko and Boyd [21]. Two sets of state-to-state transition rates are constructed in the QCT work. First, a simplified, pairwise Hulbert–Hirshfelder (HH) PES [24] is applied. The PES supports a maximum of 36 vibrational states and 223 rotational levels for the electronic ground-state O_2. This simplified HH PES is computationally less expensive than a more accurate PES. Second, an accurate many-body PES is adopted. The Varandas and Pais [25] PES generates 47 vibrational states and a maximum of 236 rotational levels for electronic ground-state molecular oxygen. These QCT results have been integrated in order to create a vibrational relaxation parameter relation that is in the form of the Landau–Teller theory formulation. Equation (6) presents the curve fit form of the vibrational relaxation parameter for the QCT based results:

$$P\tau_v = (ax^3 + bx^2 + cx + d) \times 10^{-8}, \qquad x = T/10000 \ \text{atm-s} \tag{6}$$

Table 1 summarizes the curve fit coefficients for each PES.

Figure 1 compares the O_2–O vibrational relaxation times from different methods. The O_2–O_2 vibrational relaxation time is also

Table 1 Vibrational relaxation curve fit coefficients obtained from QCT analyses

PES	a	b	c	d
2T HH PES	-4.407×10^{-6}	−0.005662	0.5433	0.08702
2T Varandas PES	2.304×10^{-3}	−0.07254	1.245	1.70

shown for reference. The O_2–O Park curve fit of the experimental data using the MW dependence [4] matches up well with the data by Breen et al. [3] only in the temperature range between 1000 and 3500 K. Above this temperature, the O_2–O MW relaxation time significantly underestimates the QCT data. In fact, the QCT results deviate from the Landau–Teller temperature dependence. The O_2–O system does not adhere to the STS transition assumptions of Landau–Teller theory; however, using a vibrataionl relaxation time to represent the internal energy evolution can capture the behavior appropriately [6]. The vibrational relaxation time, derived from the QCT rates based on the HH PES, slightly underestimates the data of Breen et al. This is because of the crude representation of the potential well in the HH PES, which appears to be too deep and wide, compared to that of the Varandas and Pais [25]. However, each PES demonstrates a similar tendency in vibrational relaxation time behavior.

2. *Dissociation Rate Coefficient*

In the 2T model, the dissociation process is generally represented by the Arrhenius-type temperature dependence. The effect of vibrational nonequilibrium is modeled by changing the controlling temperature to the geometrically averaged temperature of the translational and vibrational temperature ($T_a = \sqrt{TT_v}$) as proposed by Park [1]. The QCT results of Andrienko and Boyd [21] suggest that using the quasi-steady state (QSS) dissociation rate could be a more accurate way to model the dissociation process for O_2–O. The final dissociation model investigated in this work is the QCT-based QSS dissociation rate. As a note, this method is controlled by the translational temperature because of the QSS derivation [21] of the rates, and QSS is defined as the state at which the population rate of change is equal to zero. The Arrhenius form is shown in Eq. (7):

$$k_d = AT_a^B \exp(-C/T_a), \qquad \mathrm{cm}^3/\mathrm{s} \tag{7}$$

Additionally, the Arrhenius coefficients associated with the various models are summarized in Table 2.

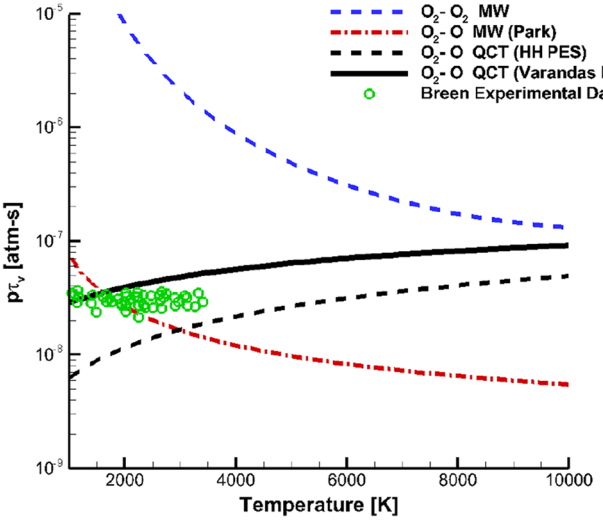

Fig. 1 O_2 – O and O_2 – O_2 vibrational relaxation times.

Table 2 Arrhenius parameters of dissociation reaction (the preexponential factor is in $\mathrm{cm}^3/\mathrm{s/mol}$)

Model	A	B	C	T_a
2T MW/Park	1.00×10^{22}	−1.5	59500	$\sqrt{TT_v}$
2T HH	1.170×10^{18}	−0.512	60650.0	$\sqrt{TT_v}$
2T Varandas	1.725×10^{18}	−0.4037	60540.0	$\sqrt{TT_v}$
2T QSS	9.0×10^{22}	−2.2	65000	T

Table 3 Curve fit parameters for vibrational energy loss coefficient due to dissociation

System	A	B	C
O_2–O_2	0.3216	−0.8362	0.9020
O_2–O	0.4505	−1.1294	0.8699

3. *Vibrational Energy Loss Due to Dissociation*

When a molecule dissociates, its vibrational energy is removed and converted into translational energy, and the loss of internal energy must be accounted for in the model. Since the dissociating molecule could be at a low vibrational state or a high vibrational state, an assumption must be made as to an average vibrational energy loss due to dissociation. It is customary to use a fraction C_{VD} of the dissociation energy to describe this vibrational energy loss. Physically, the average loss of vibrational energy is a complex function of translational temperature and instantaneous population of the vibrational manifold. The 2T model typically assumes that this parameter is constant. Most of the 2T approaches in the present work adopt the constant value method for C_{VD}. The work of Andrienko and Boyd [21] presents the temperature dependence for C_{VD}. The C_{VD} temperature dependence has been curve fit to the form of Eq. (8) with the coefficients presented in Table 3. Note that the work has assumed that the governing temperature for this quantity is the translational temperature. This assumption does not capture the vibrational population effects on C_{VD}; however, the full dependence on the vibrational temperature and population has not been captured in a compact form. Additionally, the C_{VD} parameter does not change much during intensive dissociation phases [21]. The present work focuses on postnormal shock conditions that contain significant dissociation, so the translational temperature formulation of C_{VD} is an acceptable assumption,

$$C_{\mathrm{VD}} = Ax^2 + Bx + C, \qquad x = T/10000 \tag{8}$$

A study was conducted using a temperature-dependent C_{VD} modeling approach that showed no accuracy difference when compared to the constant value approach. However, it is suggested that the model be incorporated into current models for its physical accuracy. The approach does not affect the computational expense of the simulation and provides a more physical representation even if the benefit of the model is not observable in these test cases.

B. State-to-State Model

The conservation of vibrational energy in the STS model is formulated for each vibrational energy level. This approach significantly increases the number of equations to be solved; however, it eliminates highly averaged parameters such as τ_v and C_{DV} that can vary drastically for each vibrational energy level. Additionally, the conservation equations for species densities, given in Eq. (1) can be omitted. The system of equations for the STS model in this case accounts for the conservation of momenta and transrotational energy as well as for number density of individual vibrational states. The latter has the appearance

Table 4 Summary of low- and high-fidelity models of nonequilibrium thermochemistry, adopted in the present work

		O_2–O_2		O_2–O		
Title	Model	VT	Dissociation	VT	Dissociation	C_{VD}
2T–MW/Park	2T	MW	Park	MW	Park	Constant
2T–MW/Park/C_{VD}	2T	MW	Park	MW	Park	$f(T)$
2T–MW/QSS/C_{VD}	2T	MW	Park	MW	QSS	$f(T)$
2T–HH	2T	MW	Park	HH QCT	Constant	— —
2T–Varandas	2T	MW	Park	Varandas QCT	Constant	— —
STS–QCT Varandas	STS	FHO	FHO	Varandas QCT	— —	— —

$$\frac{\partial n_v}{\partial x} = \sum_s (R_{v,s} n_O^2 n_s - D_{v,s} n_v n_s) + \sum_s (K_{v',v} n'_v n_s - K_{v,v'} n_v n_s), \qquad v = 0, \ldots, v_{\max} \quad (9)$$

where summation takes place over projectile species, in the present case, O_2 and O. The final results are provided in a curve fit form as shown in Eqs. (10) and (11) for bound–bound and bound-free transition rate coefficients,

$$K_{v,v'} = 10^{-12} \times \exp[A_{v,v'} + B_{v,v'}/\log(T/1000) + C_{v,v'} \log(T/1000)], \qquad \text{cm}^3/\text{s} \quad (10)$$

$$D_v = A_v T^{B_v} \exp(-C_v/T), \qquad \text{cm}^3/\text{s} \quad (11)$$

The vibrational-translational (VT) transition rates for the O_2–O_2 system are taken from FHO analysis [16,21]. These rates are used in a postnormal shock calculation using the master equation approach outlined in [8]. The governing parameter for the FHO model is the exponential potential parameter α. Previous FHO [16] work for oxygen has shown that the value of α is near 4.0 Å^{-1}. This value is based on the comparison of vibrational relaxation time in pure oxygen obtained by means of the master equations with the experimental data. The present work investigates the sensitivity of the FHO α parameter used in the O_2–O_2 STS rates, and α parameters of 3.8, 4.0, and 4.2 are studied. A set of vibration–vibration transition rates has also been generated for O_2–O_2 collisions; however, preliminary runs of the STS model have not revealed any significant importance of this energy transfer mechanism at the given range of translational temperatures. The O_2–O_2 state-specific dissociation rates are determined by scaling the O_2–O rates using the global dissociation rates of Bortner [21,26]. It should be noted that vibrational temperature is used for experimental comparisons in the presented work. The vibrational temperature is calculated by taking the vibrational energy from the STS simulation and deducing a Boltzmann equivalent vibrational temperature.

Table 4 summarizes the modeling approaches that are investigated in the present work.

III. Results

The postnormal shock flow calculations are carried out for an existing set of shock tube experiments conducted by Ibraguimova et al. [27]. The flow conditions for the test cases are summarized in Table 5. All flow conditions have a pure O_2 freestream composition. The set of test cases represents a relevant range of conditions that might be experienced by a hypersonic vehicle.

Table 5 Summary of flow conditions investigated [27]

Test case	Shock velocity, km/s	P_1, torr	T_1, K	T_2, K
C1	3.07	2.0	295	5300
C2	3.95	1.0	295	8620
C3	4.44	0.8	295	10,820

A. Two-Temperature Model

The results for the 2T model are separated into two subsections: VT energy transfer and dissociation and the QSS phase. These subsections aim to isolate the various aspects of modeling that are investigated.

1. *VT Energy Transfer and Dissociation*

First, the conventional 2T model (2T–MW/Park) is compared with the newly derived 2T QCT-based models (2T–HH and 2T–Varandas). The models are also evaluated against the experimental results from [27].

Figures 2 and 3 show profiles of temperature and composition for the C1 case. Time begins with the passage of the shock wave. This case corresponds to mild vibrational nonequilibrium with a relatively low postshock temperature. At these conditions, vibrational relaxation occurs much more quickly than chemical transformation. Hence, the widely used QSS assumption about separation of these two processes is valid. All 2T models predict a similar rate of vibrational relaxation and dissociation. The mild translational temperature leads to a very small amount of atomic oxygen being present during the vibrational relaxation. At the moment of the onset of dissociation, the flow contains only 2–3% of atomic oxygen, and so the O_2–O_2 collisions govern vibrational relaxation. Since all 2T models use the same MW coefficients for O_2–O_2 collisions, it is expected that they all have similar behavior. Only slight differences are observed after 1.0 μs due to the start of dissociation, and thus the presence of atomic oxygen. The results from all models generally fall within the error bars of the experimental data.

Figures 4 and 5 show the temperature profiles and the composition evolution for the case C2. For this condition, there is dissociation before the end of vibrational relaxation. This introduces atomic oxygen in the amount of approximately 10%, and differences are seen in the prediction of the different models. Specifically, after 0.2 μs, the behavior differs significantly due to the different dissociation models. The higher-fidelity 2T–Varandas model agrees better with the Park model in terms of the dissociation rate, compared to the 2T–HH model. The first two models predict faster dissociation and, hence, a lower vibrational temperature after 0.2 μs. However, all 2T models underestimate T_v during the phase of active dissociation in the C2 case. One may conclude that the global rates incorporated in their present form in the 2T model need adjustment to match the experimental data.

The C3 case corresponds to the highest degree of nonequilibrium among all studied cases. The temperature and species profiles for the model results for C3 are shown in Figs. 6 and 7. All 2T models fail to accurately describe thermal relaxation. Specifically, the 2T models underestimate the experimental data. The flow contains between 15 and 20% of atomic oxygen at the moment when T and T_v become equal. From the slope of vibrational temperature, one can conclude that the location of $T = T_v$ is captured incorrectly by the 2T models, but due to large error bars, some experimental points fall within theoretical predictions. As in the C2 case, the 2T–Park and 2T–Varandas models predict similar rates of dissociation, and the 2T–HH model with the lower-fidelity PES gives the slowest dissociation rate.

One may conclude from cases C1–C3 that the new vibrational relaxation time, generated by the QCT analysis of the O_2–O system, has little influence on the vibrational temperature during the early phase of relaxation if incorporated in a low-fidelity 2T model. This is

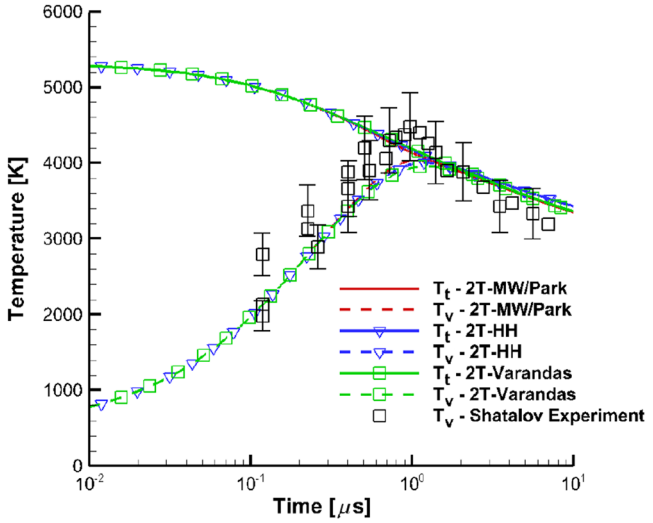

Fig. 2 Temperature profiles evaluating 2T variants, C1 case.

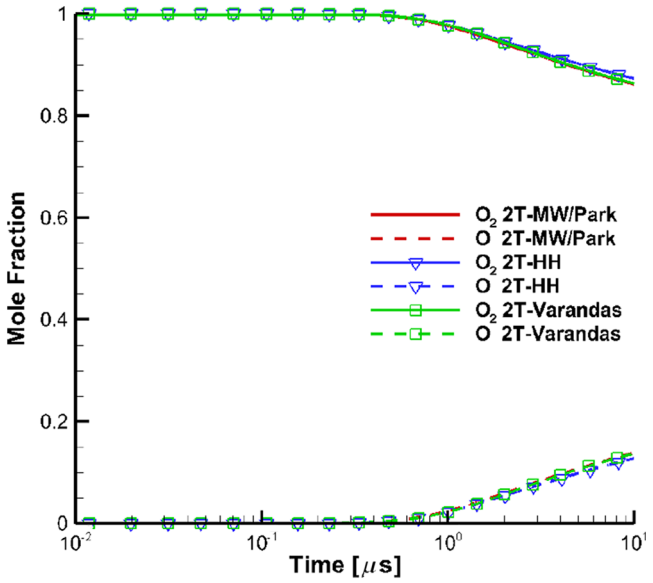

Fig. 3 Composition profiles evaluating 2T variants, C1 case.

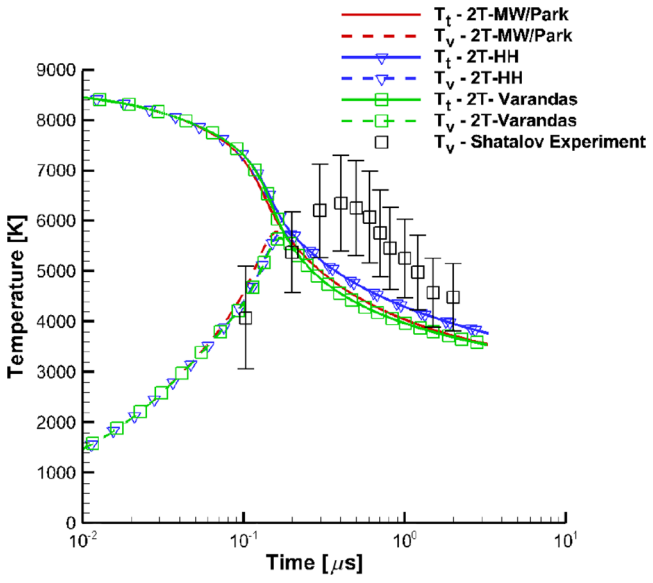

Fig. 4 Temperature profiles evaluating 2T variants, C2 case.

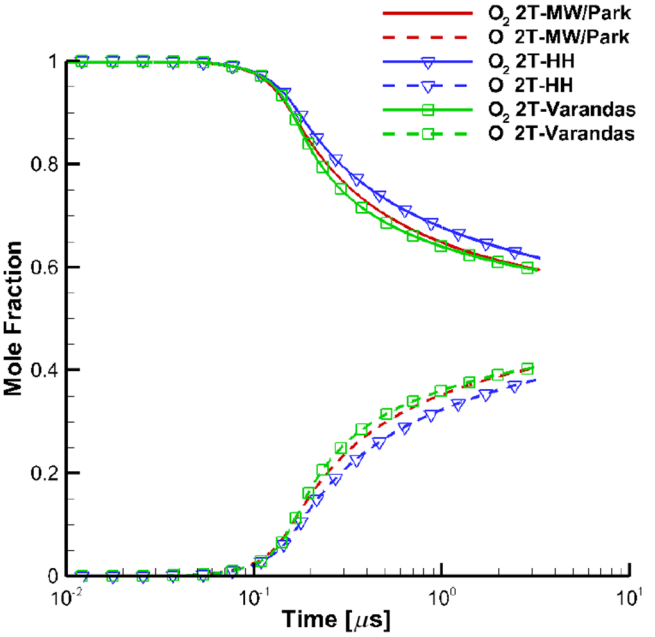

Fig. 5 Composition profiles evaluating 2T variants, C2 case.

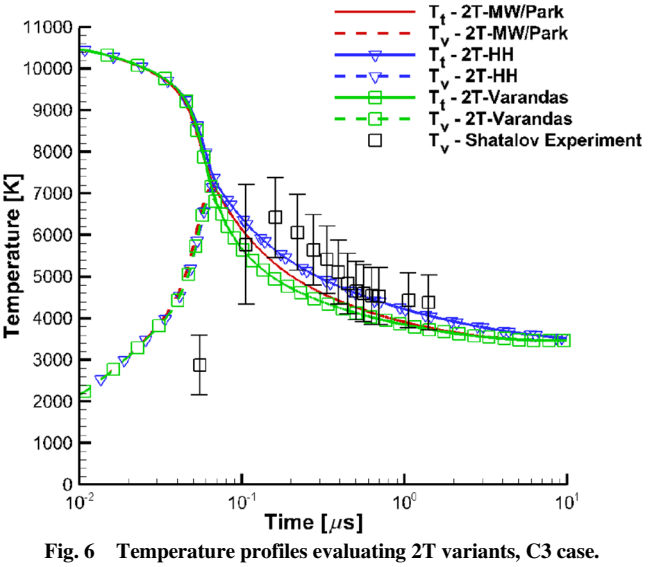

Fig. 6 Temperature profiles evaluating 2T variants, C3 case.

not surprising, since all experimental runs initially contained only pure diatomic oxygen. However, the importance of atomic oxygen for vibrational relaxation was demonstrated in [21] for cooling flows even with similar initial composition.

Additionally, it is clear that the use of thermal-equilibrium dissociation rate coefficients obtained from the QCT simulations with the Park model of vibration–dissociation coupling underestimate the vibrational temperature during active dissociation. This indicates that the actual, effective dissociation rate should be lower than what is presently used. The following section expands discussion on this matter.

2. *QSS Dissociation Rate Coefficient*

Because of the incomplete thermalization of the vibrational ladder, the dissociation rate during the QSS phase is lower than that estimated at thermally equilibrium conditions. The ratio of equilibrium and QSS rate coefficients is approximately 3 according to Park [28]; however, for O_2–O, this ratio is found to increase rapidly at high temperature due to inefficient vibrational relaxation at these conditions. The QSS rate coefficients can be derived from the complete set of bound–bound and bound-free transition rate

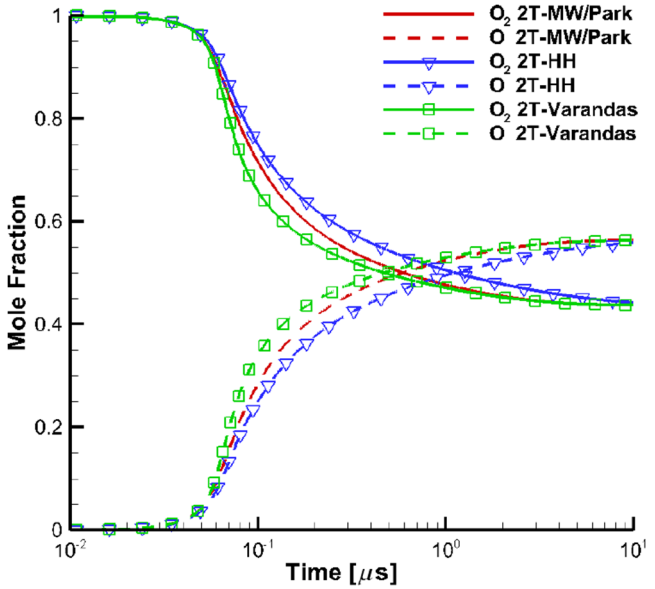

Fig. 7 Composition profiles evaluating 2T variants, C3 case.

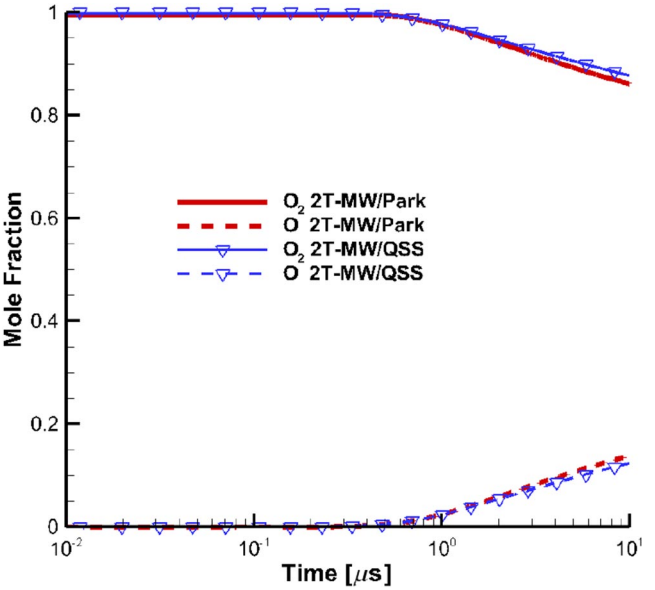

Fig. 9 Composition profiles evaluating QSS dissociation rates, C1 case.

coefficients by solving the system of master equations with the additional constraint of $\partial n_v/\partial t = 0$.

As mentioned in the modeling description section, the work of Andrienko and Boyd [6] demonstrated that using the QSS dissociation rate coefficients could be more accurate than the equilibrium rates typically used in the 2T model. In the present work, the effect of using the QSS dissociation rate coefficients is investigated for the experimental cases in [27]. Since the QSS dissociation rate represents the actual rate of depletion, no vibration–dissociation coupling, such as Park's model, is necessary.

The MW equation is used for the vibrational relaxation modeling, while the two different methodologies for the dissociation rate are compared. It should be noted that the QSS rates are known only for the O_2–O system. Since the high-fidelity QCT rates for O_2–O_2 are presently unavailable, the QSS dissociation rate for this system is not investigated in the present work. Other rates are available for O_2–O_2; however, the present work focuses on the newly available QCT rates for O_2–O.

The results for C1 are shown in Figs. 8 and 9. The effect of using the QSS dissociation rates for O_2–O are minimal for this test case. A slight difference in the results can be seen after 2 μs, once a sufficient atomic number density is present in the flowfield. The results are consistent with the fact that the QSS dissociation rate is less than the equilibrium dissociation rate.

The results for C2 are shown in Figs. 10 and 11. The model with the QSS dissociation rate coefficients incorporated clearly shows the desired increase of vibrational temperature toward better agreement with the experimental data. However, even with the improvement, this QSS model still lies slightly below the error bands of the experimental data. This is due to an incorrect capturing of vibrational relaxation, which follows from the misplacement of the maximum of T_v. Specifically, the 2T models appear to reach the maximum vibrational temperature more quickly than the experimental data, leading to a different profile than the experimental results.

Figures 12 and 13 show the results for the C3 case. The QSS dissociation rate model achieves better agreement with the experimental results than the conventional 2T–Park model. The QSS approach remains within the experimental error band for the majority of the relaxation process. However, it is clear that neither of 2T models captures the early behavior of thermalization. The vibrational relaxation for the 2T models appears to happen too rapidly at the beginning of the process.

In summary, the QSS dissociation rate coefficients provide better agreement with experimental data for these postshock test cases. The

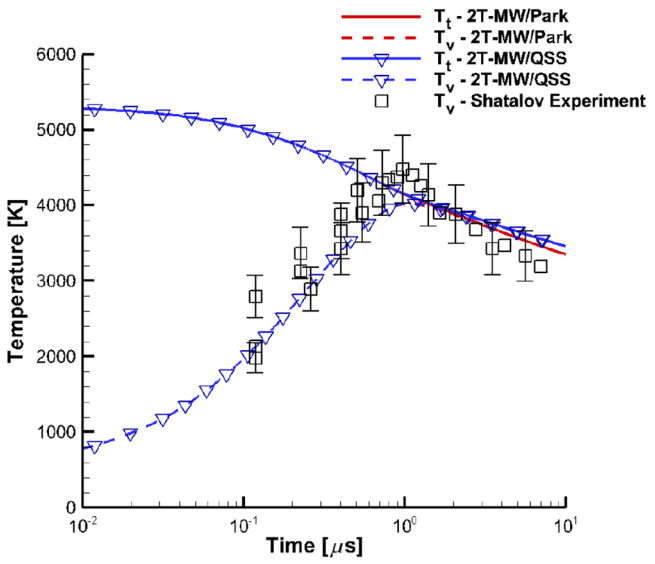

Fig. 8 Temperature profiles evaluating QSS dissociation rates, C1 case.

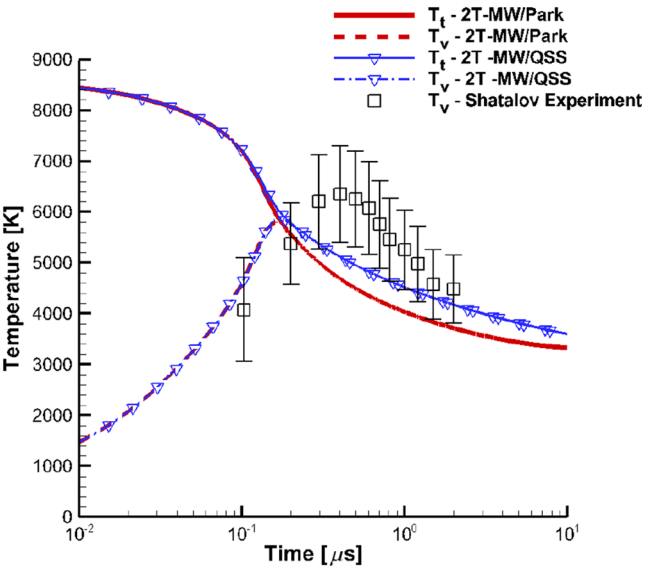

Fig. 10 Temperature profiles evaluating QSS dissociation rates, C2 case.

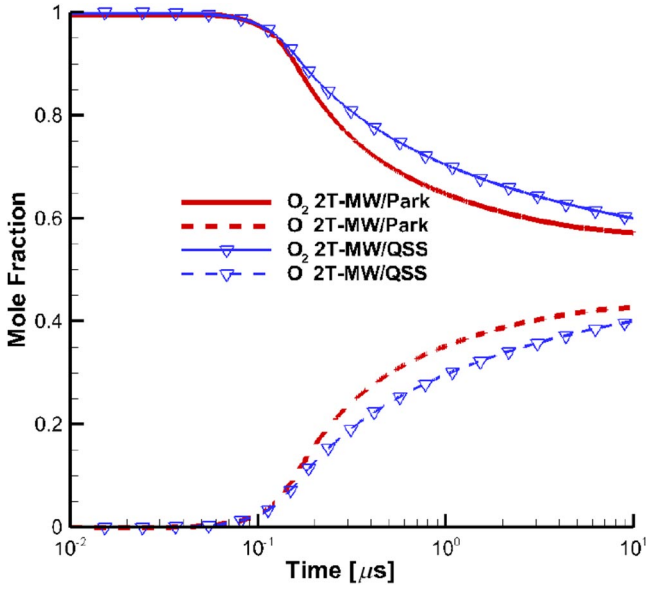

Fig. 11 Composition profiles evaluating QSS dissociation rates, C2 case.

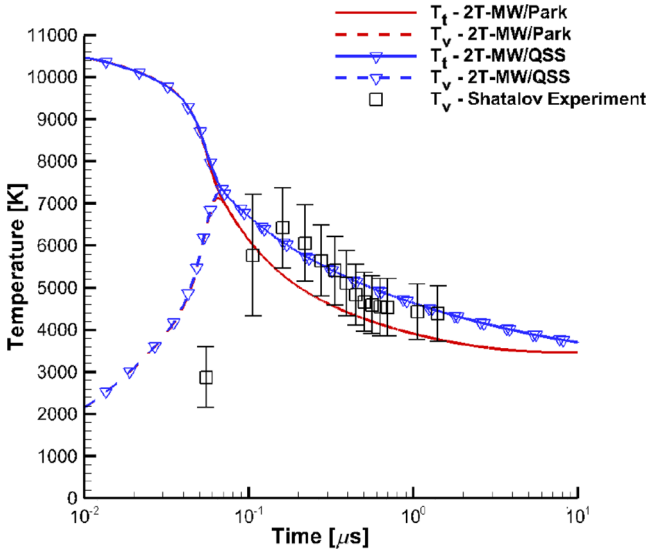

Fig. 12 Temperature profiles evaluating QSS dissociation rates, C3 case.

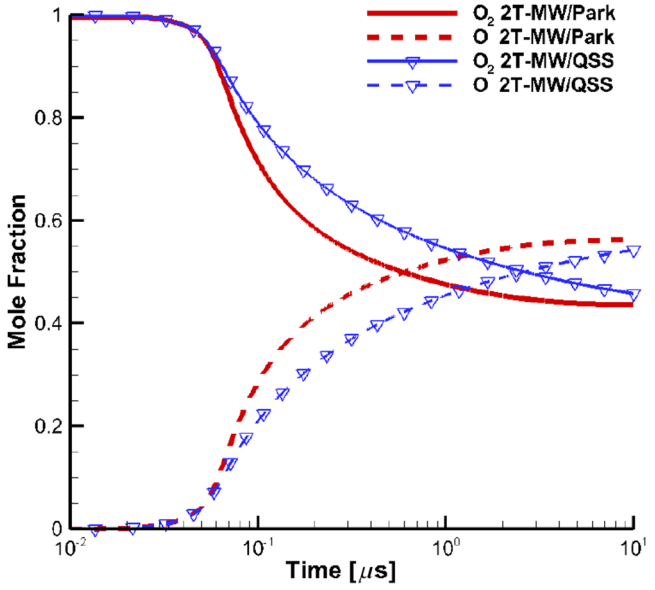

Fig. 13 Composition profiles evaluating QSS dissociation rates, C3 case.

QSS dissociation rates described in the presented work for are for the O_2–O system. However, the 2T modeling is still not able to completely capture the behavior observed in the experimental data. Specifically, the 2T models have difficulty capturing the maximum vibrational temperature and the location of transvibrational equilibrium.

B. State-to-State Model

The STS results section is separated into two portions. First, the sensitivity of the repulsive parameter $\boldsymbol{\alpha}$ assumed by the FHO model is investigated to evaluate its influence on the O_2–O_2 STS rate coefficients and consequently on the overall solution. Next, the vibrational temperature and species profiles generated by the STS model are compared with those from the 2T models and the experiments [19].

1. O_2–O_2 *FHO Parameter Sensitivity*

The STS rates use the FHO method that assumes the exponential repulsion in the O_2–O_2 system defined by parameter α. In the present work, the test cases using α values of 3.8, 4.0, and 4.2 are simulated. Previous work has shown that the exponential potential parameter is in this range near 4.0 $Å^{-1}$ [21]. In this section, the O_2–O STS model adopts the QCT rates obtained from the Varandas potential.

Figure 14 presents the temperature profiles for the parametric study of α. As would be expected for the pure O_2 freestream, the α parameter has a strong influence on the solution since the early vibrational–translational behavior is primarily governed by O_2–O_2 collisions. A value of 3.8 has slower relaxation than the solutions obtained with the values of 4.0 and 4.2 for the entire relaxation process. After the vibrational temperature reaches the maximum, the results begin to coalesce. The later relaxation behavior is essentially identical between the various values of α. Even with the notable differences in behavior, all of the results fall within the spread of the experimental data.

Figure 15 presents the temperature profiles for C2. This case shows a similar influence of α on the temperature results. The faster relaxation due to higher temperatures and the faster introduction of O atoms from dissociation slightly reduce the variation due to α differences in comparison to C1.

Figure 16 presents the C3 temperature profiles. The application of the FHO rates for this case clearly shows the benefit of the STS model over the 2T model in terms of the better agreement of T_v for the early stage of relaxation. At these elevated translational temperatures, the α influence is slightly mitigated by the quicker introduction of O atoms. All the results miss the first experimental

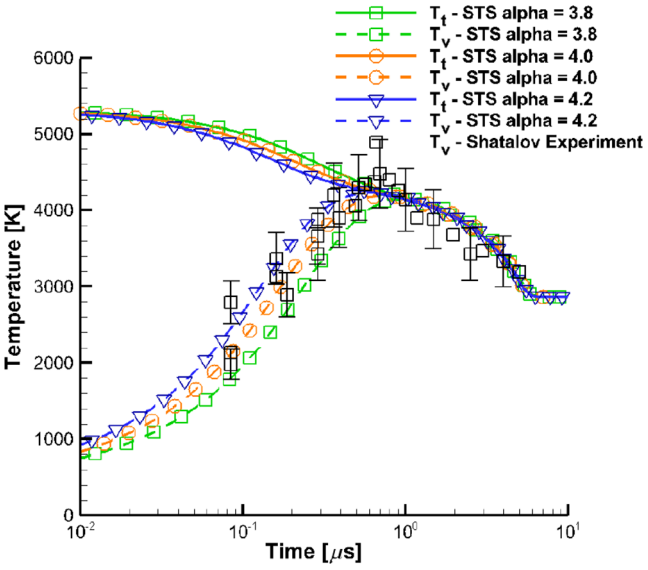

Fig. 14 Temperature profiles evaluating the effect of α, C1 case.

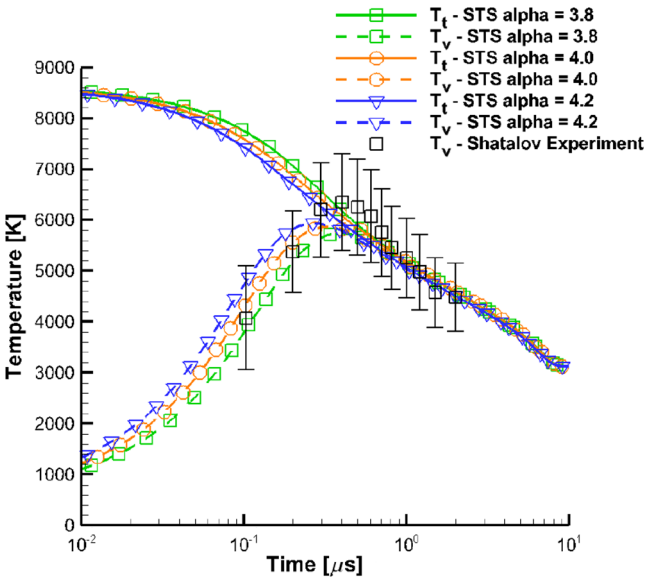

Fig. 15 Temperature profiles evaluating the effect of α, C2 case.

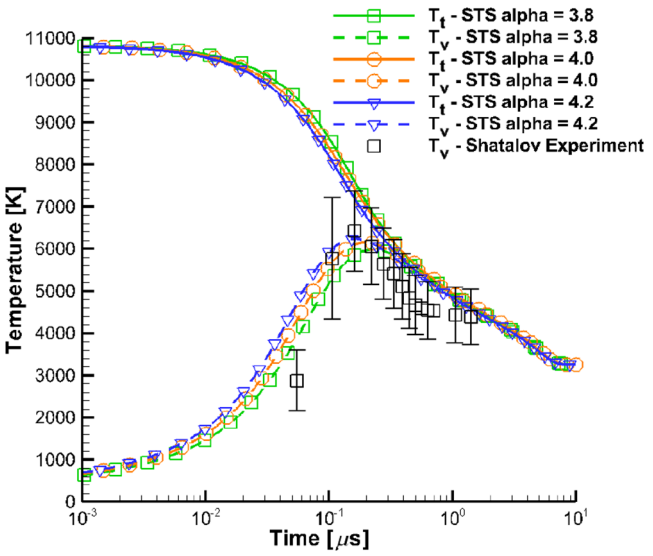

Fig. 16 Temperature profiles evaluating the effect of α, C3 case.

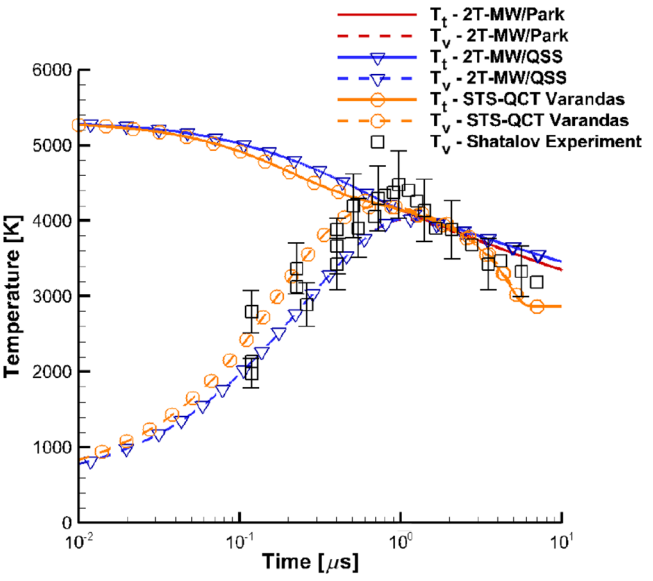

Fig. 17 Temperature profiles evaluating STS, C1 case.

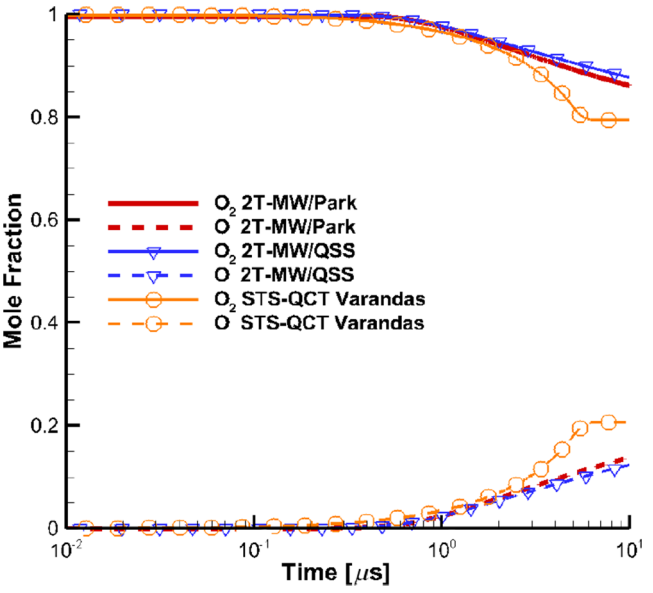

Fig. 18 Composition profiles evaluating STS, C1 case.

point, but the α value of 3.8 is closest to capturing the first few experimental points. The present work adopts the α value of 4.0 for the rest of the work in the paper.

In summary, the different values of α have a pronounced influence on the O_2–O_2 behavior. However, this effect is still smaller than the difference in T_v between the STS and 2T models. This indicates a great potential of STS models for the accurate description of the temperature and species profiles behind shock waves.

2. *2T and STS Models Comparison*

The results in this section focus on comparing the current 2T models with the high-fidelity, STS modeling approach and with the experimental data. The previous section showed that the QSS dissociation rate coefficients provide better agreement with the experimental data when incorporated in the 2T model. The improved 2T approach used for comparison in this section is the 2T–MW/QSS modeling approach. The STS–QCT Varandas method represents the highest level of fidelity investigated in this study.

Figure 17 presents the evolution of temperature for the three modeling approaches for C1. There is a fundamentally different vibrational temperature profile between the STS and 2T approaches. The most notable differences are in the early vibrational relaxation phase and also the time at which the maximum vibrational temperature is reached. The STS model relaxes more rapidly than the 2T models and reaches the maximum vibrational temperature first. The VT energy exchange by means of the STS model results in a noticeable difference in the profiles of translational temperature. Another important feature of the STS approach is a much faster convergence of temperature to the equilibrium value, compared to the 2T models. Overall, the STS model matches the experimental data very well. Figure 18 shows the difference in the composition evolution for the three models. The rapid thermalization of vibrational and translational temperatures predicted by the STS model corresponds to the active generation of atomic oxygen in the flow, which is known to be much more effective for O_2 dissociation compared to diatomic oxygen [29].

Figures 19 and 20 present the evolution of the vibrational state population distribution for the STS model. The Boltzmann distributions plotted represent a temperature equivalent distribution for that given time. The first time location ($t = 0$ μs) represents the vibrational population distribution just before the shock passage. Initially, the flow is in equilibrium, and the actual distribution does

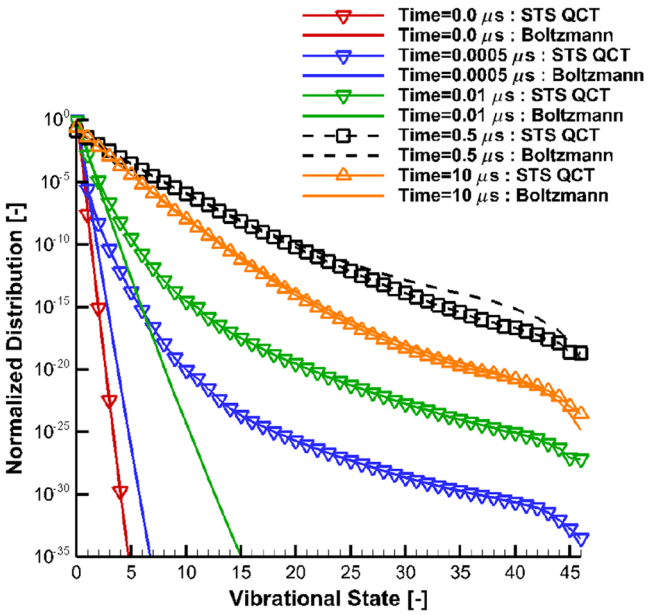

Fig. 19 Vibrational population distribution evolution, C1 case.

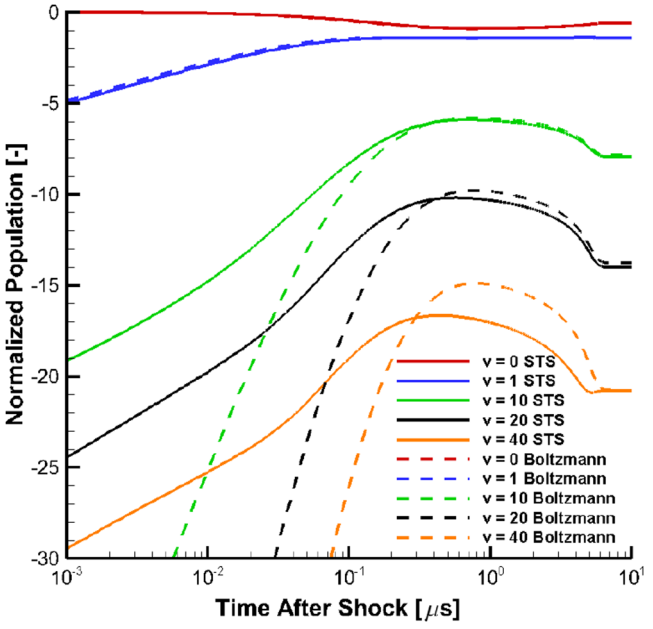

Fig. 20 Vibrational state population evolution, C1 case.

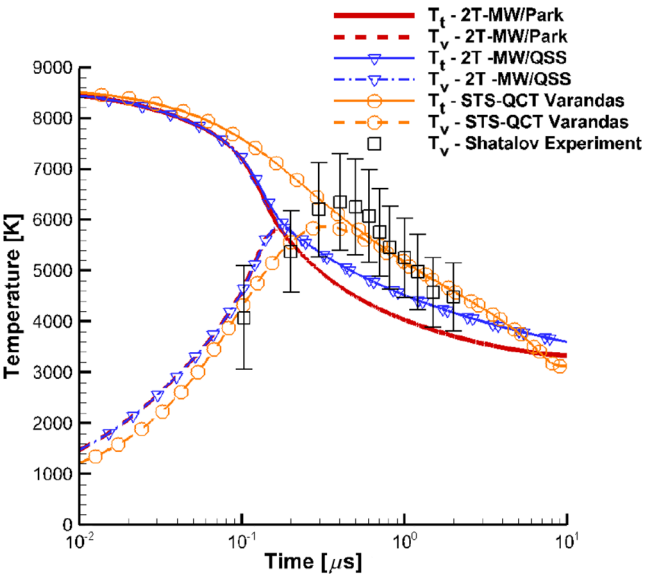

Fig. 21 Temperature profiles evaluating STS, C2 case.

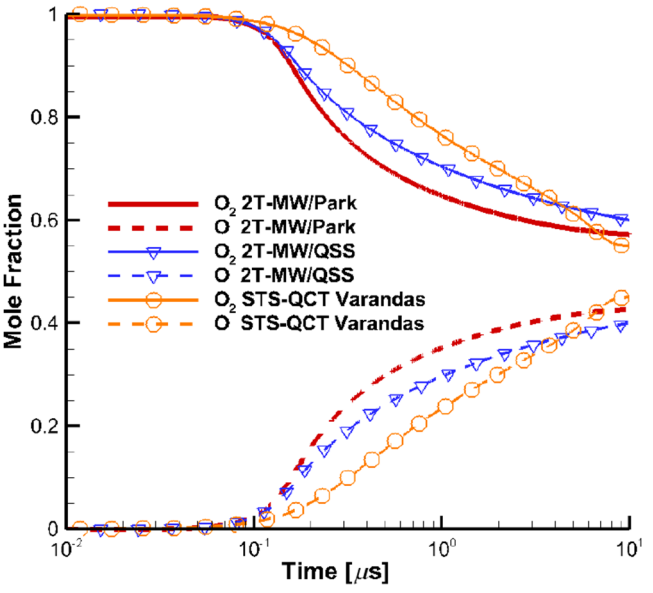

Fig. 22 Composition profiles evaluating STS, C2 case.

not deviate from the Boltzmann distribution. Once the shock passes, the distribution strongly deviates from the Boltzmann population before the onset of dissociation. The vibrational state population plots show that during the early vibrational relaxation phase all the states higher than $v = 3$ are strongly overpopulated. In contrast, the $v = 1$ state shows a slight underpopulation relative to the Boltzmann distribution. The non-Boltzmann behavior shown in the population distribution during the relaxation process is mainly attributed to the ability of the STS model to account for multiquantum transitions.

As the relaxation process continues, a change in slope of the population for $v = 10$, 20, and 40 can be observed in Fig. 20 around 0.02 μs. This slope change is an indication that the dissociation process has started and of the presence of the oxygen atoms that lead to faster relaxation (O_2–O collisions). The dissociation is dominant in the higher vibrational states ($v > 25$) and, as the dissociation process increases, causes an underpopulation in these higher vibrational states. This large amount of dissociation from the higher vibrational states results in a smaller amount of energy being removed from the internal modes and a higher vibrational temperature compared to the 2T models. Additionally, the O_2–O collisions dominate the late phase of the chemical thermalization due to the efficient energy transfer of the collision. This attribute is realized in the rapid approach to equilibrium in the late phase ($t > 0.2$ μs) when compared to the 2T model that implicitly assumes a Boltzmann distribution.

Figures 21 and 22 present the evolution of temperature and composition for C2. The difference in the behavior between the STS and 2T models is more significant, compared to C1. Unlike the 2T models, the STS approach is capable of describing the correct nonmonotonic behavior of the vibrational temperature and predicts the location of the T_v maximum. The STS solution is well within the experimental bars, and one can say that the higher-fidelity model clearly shows an improvement over the simple 2T models.

Figures 23 and 24 present the vibrational population distribution for C2. The general behavior of the vibrational ladder is quite similar to that for C1. However, two aspects are different. First, the excited states deviate strongly from the equilibrium value compared to the C1 case. Second, the lower vibrational states ($v > 23$) become depleted

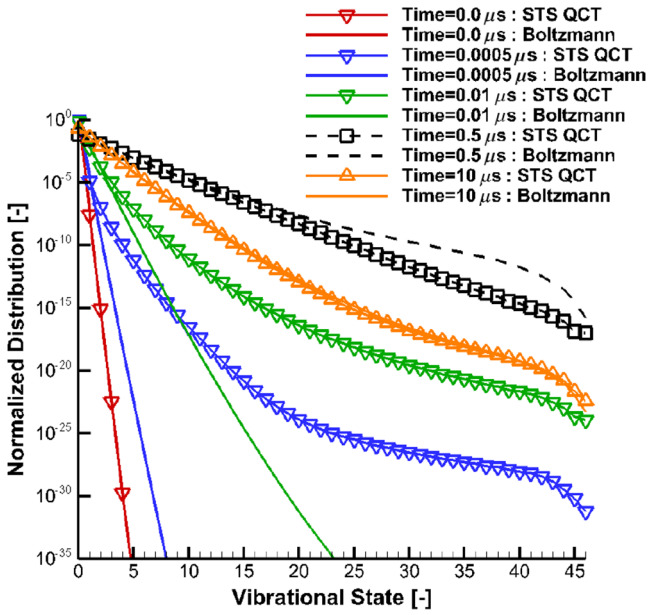

Fig. 23 Vibrational population distribution evolution, C2 case.

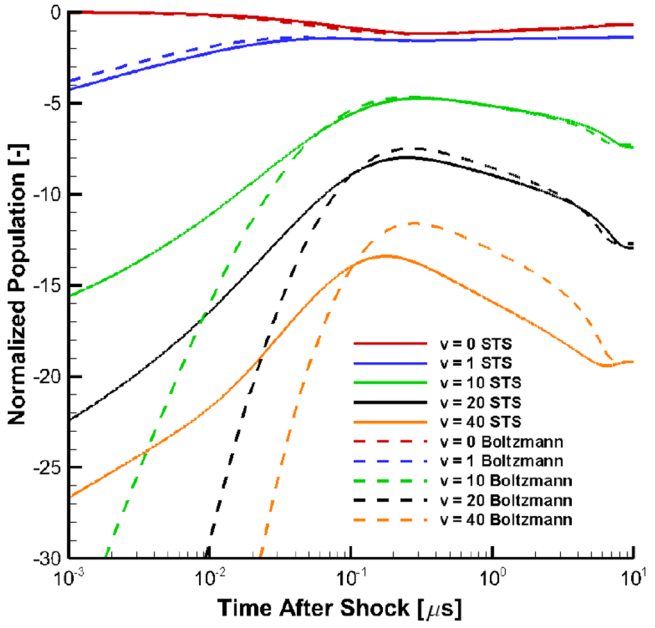

Fig. 24 Vibrational state population evolution, C2 case.

during active dissociation. This means that at stronger nonequilibrium conditions the probability density function shifts toward the low-lying states [6].

The profiles of the vibrational temperature and species mole fraction for C3 are given in Figs. 25 and 26. It is important to note than the STS model allows the accurate description of the phase of initial vibrational relaxation and clearly performs better than the 2T model. The location of the maximum vibrational temperature and the duration of the dissociation phase is captured by the STS approach, too. In other words, the C2 and C3 cases show the superior accuracy of the STS model for describing thermal nonequilibrium flows of oxygen. The profiles of species for case C3 are similar to those of case C2: the initial rate of atomic oxygen production is lower; however, the large slope leads to a faster chemical equilibrium.

The state-resolved population of the vibrational ladder for C3 is given in Figs. 27 and 28. Under these conditions, vibrational states with $v > 20$ are noticeably affected by the dissociation.

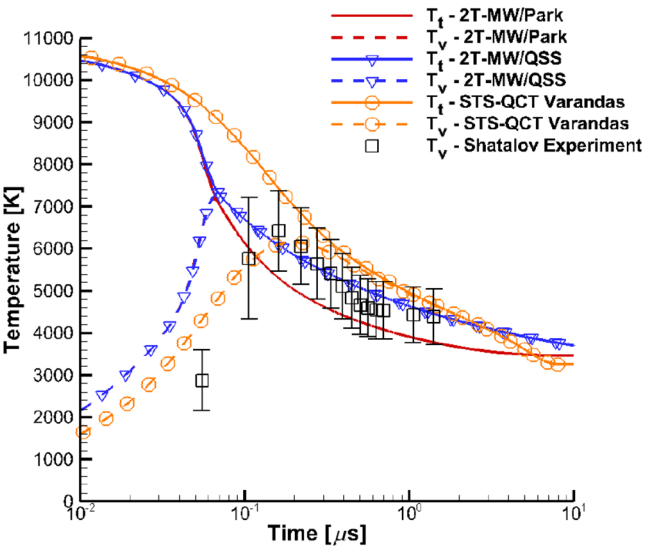

Fig. 25 Temperature profiles evaluating STS, C3 case.

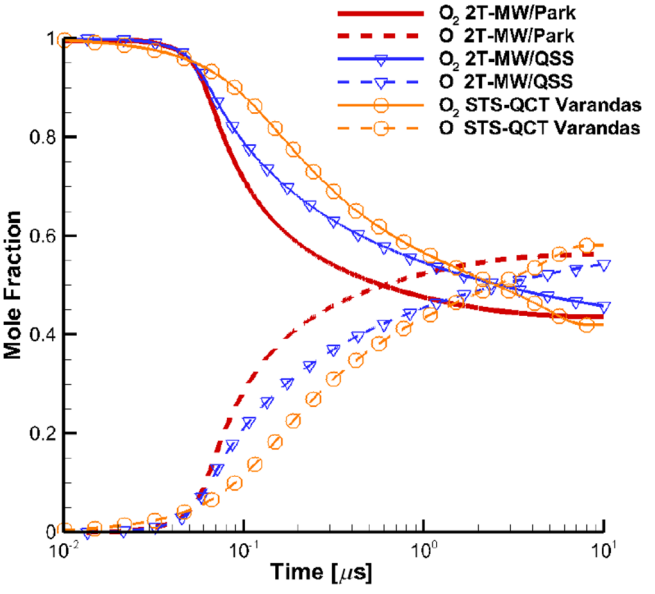

Fig. 26 Composition profiles evaluating STS, C3 case.

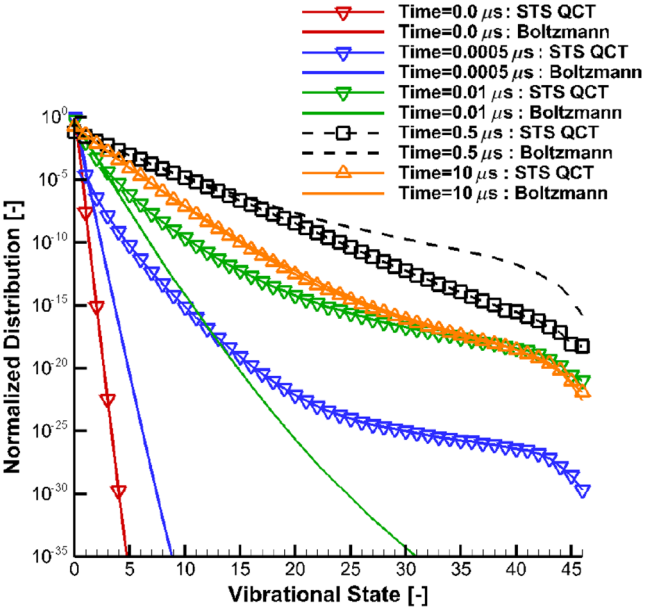

Fig. 27 Vibrational population distribution evolution, C3 case.

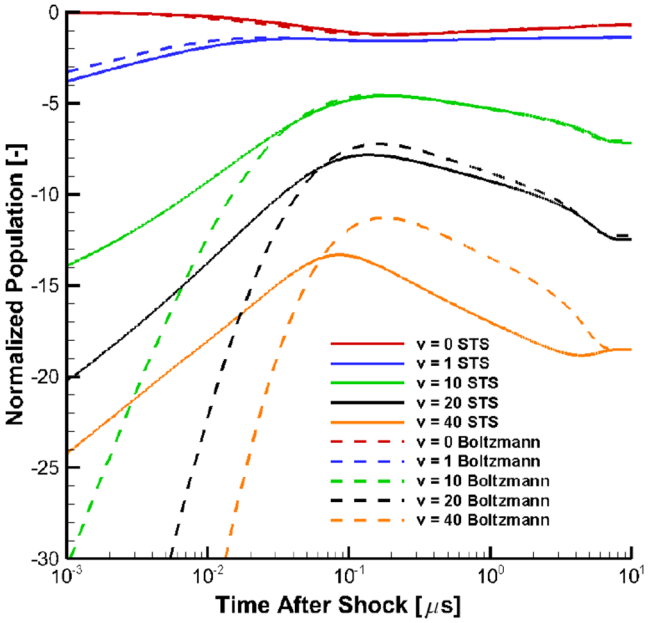

Fig. 28 Vibrational state population evolution, C3 case.

IV. Conclusions

Vibrational nonequilibrium and dissociation models of varying fidelity were compared to several sets of experimental data obtained in a shock tube facility. First, the conventional two-temperature model was presented with potential improvements based on recently available quasi-classical trajectory results for the O_2–O system. Namely, the vibrational relaxation time, quasi-steady-state (QSS) dissociation rate coefficients, and the temperature-dependent coupling between the vibrational mode and dissociation were implemented.

The results of two-temperature (2T) model simulations suggested that the new O_2–O vibrational relaxation time has little effect on the evolution of the vibrational temperature immediately behind the shock front. This could be attributed to the fact that the experimental cases contained pure diatomic oxygen as the initial conditions. In vibrationally nonequilibrium flows with a significant amount of atomic oxygen, the effect of the fast O_2–O vibrational quenching is expected to be more pronounced. However, one should note that the 2T models were unable to provide an accurate description of vibrational temperature before the onset of dissociation in the shock tube flows.

The implementation of the global QSS dissociation rate coefficients in the 2T model without coupling by means of an effective temperature according to the Park model provided a better agreement of the computed vibrational temperature with the experimental data when the dissociation process was active. This observation confirms the usefulness of the master equation analysis that generates highly averaged parameters that can be adopted by simpler models. Additionally, no pronounced effect of the variable vibration–dissociation coupling coefficient was found, potentially due to the relatively low pressures and temperatures behind the shock front. However, as a matter of principle, the inclusion of this temperature dependence is recommended since it is more physically representative and does not introduce any additional computational cost.

Finally, the present work incorporated a new set of O_2–O state-specific rate coefficients in the higher-fidelity model. It is important to note that this step allowed the correct prediction of the vibrational temperature before the onset of dissociation as well as during active chemical processes. It can be concluded that the present state-to-state (STS) model has higher predictive capabilities compared to the 2T model, since the state-specific model does not employ any empirical parameters. These improvements can be clearly observed for the C2 and C3 cases that correspond to a higher shock velocity and higher degree of nonequilibrium. Still, it is highly desired to obtain experimental data with smaller uncertainty bars for a more detailed assessment of STS models.

Acknowledgments

The authors gratefully acknowledge funding for this work through the U.S. Air Force Office of Scientific Research grant FA9550-12-1-0483. K. N. would like to thank Jae Gang Kim for a code that would evolve into the flow solver used in this work.

References

[1] Park, C., *Nonequilibrium Hypersonic Aerothermodynamics*, Wiley, New York, 1989, pp. 89–92, 306–316.

[2] Millikan, R. C., and White, D. R., "Systematics of Vibrational Relaxation," *Journal of Chemical Physics*, Vol. 39, No. 12, 1963, pp. 3209–3213. doi:10.1063/1.1734182

[3] Breen, J., Quy, R., and Glass, G., "Vibrational Relaxation of O_2 in the Presence of Atomic Oxygen," *Journal of Chemical Physics*, Vol. 59, No. 1, 1973, pp. 556–557. doi:10.1063/1.1679846

[4] Kiefer, J. H., and Lutz, R. W., "The Effect of Oxygen Atoms on the Vibrational Relaxation of Oxygen," *Symposium (International) on Combustion*, Vol. 11, Elsevier, New York, 1967, pp. 67–76.

[5] Park, C., "Review of Chemical-Kinetic Problems of Future Nasa Missions. I—Earth Entries," *Journal of Thermophysics and Heat Transfer*, Vol. 7, No. 3, 1993, pp. 385–398. doi:10.2514/3.431

[6] Andrienko, D. A., and Boyd, I. A., "Rovibrational Energy Transfer and Dissociation in O^2–O Collisions," *Journal of Chemical Physics*, Vol. 144, No. 10, 2016, pp. 1–19. doi:10.1063/1.4943114

[7] Panesi, M., Jaffe, R. L., Schwenke, D. W., and Magin, T. E., "Rovibrational Internal Energy Transfer and Dissociation of $N_2(^1\Sigma_g^+)$–$N(^4S_u)$ System in Hypersonic Flows," *Journal of Chemical Physics*, Vol. 138, No. 4, 2013, pp. 1–16. doi:10.1063/1.4774412

[8] Valentini, P., Schwartzentruber, T. E., Bender, J. D., Nompelis, I., and Candler, G. V., "Direct Simulation of Rovibrational Excitation and Dissociation in Molecular Nitrogen Using an ab initio Potential Energy Surface," *45th AIAA Thermophysics Conference*, AIAA Paper 2015-474, June 2015.

[9] Kulakhmetov, M., Gallis, M., and Alexeenko, A., "Effect of $O^2 + O$ *ab initio* and Morse Additive Pairwise Potentials on Dissociation and Relaxation Rates for Nonequilibrium Flow Calculations," *Physics of Fluids*, Vol. 27, No. 8, 2015, pp. 1–0.

[10] Kim, J. G., and Boyd, I. D., "State-Resolved Master Equation Analysis of Thermochemical Nonequilibrium of Nitrogen," *Chemical Physics*, Vol. 415, No. 1, 2013, pp. 237–246.

[11] Capitelli, M., Colonna, G., and Esposito, F., "On the Coupling of Vibrational Relaxation with the Dissociation-Recombination Kinetics: from Dynamics to Aerospace Applications," *Journal of Physical Chemistry A*, Vol. 108, No. 41, 2004, pp. 8930–8934. doi:10.1021/jp048847v

[12] Kustova, E., Nagnibeda, E., and Chauvin, A., "State-to-State Nonequilibrium Reaction Rates," *Chemical Physics*, Vol. 248, No. 2, 1999, pp. 221–232. doi:10.1016/S0301-0104(99)00213-X

[13] Bellucci, V., Colonna, G., Capitelli, M., Armenise, I., Giordano, D., and Bruno, C., "Vibrational Relaxing Flow of n_2 Past an Infinite Cylinder," *Journal of Thermophysics and Heat Transfer*, Vol. 11, No. 1, 1997, pp. 27–35. doi:10.2514/2.6219

[14] Tuttafesta, M., Capitelli, M., Colonna, G., and Giordano, D., "Non-Arrhenius No Formation Rate in One-Dimensional Nozzle Airflow," *Journal of Thermophysics and Heat Transfer*, Vol. 13, No. 3, 1999, pp. 372–375. doi:10.2514/2.6448

[15] Pietanza, L. D., Colonna, G., and d'Ammando, G., "Self-Consistent Collisional-Radiative Model for Hydrogen Atoms: Atom-Atom Interaction and Radiation Transport," *Chemical Physics*, Vol. 398, No. 1, 2012, pp. 37–45. doi:10.1016/j.chemphys.2011.06.019

[16] Adamovich, I. V., MacHeret, S. O., Rich, J. W., and Treanor, C. E., "Vibrational Energy Transfer Rates Using a Forced Harmonic Oscillator Model," *Journal of Thermophysics and Heat Transfer*, Vol. 12, No. 1,

1998, pp. 57–65.
doi:10.2514/2.6302

[17] Neitzel, K., Kim, J. G., and Boyd, I. D., "Nonequilibrium Modeling of Oxygen in Reflected Shock Tube Flows," AIAA Paper 2014-2961, 2014.

[18] Truhlar, D. G., and Muckerman, J. T., "Reactive Scattering Cross Sections III: Quasiclassical and Semiclassical Methods," *Atom-Molecule Collision Theory*, Springer–Verlag, Berlin, 1979, pp. 505–566.

[19] Ibraguimova, L., Sergievskaya, A., Levashov, V. Y., Shatalov, O., Tunik, Y. V., and Zabelinskii, I., "Investigation of Oxygen Dissociation and Vibrational Relaxation at Temperatures 4000–10,800 k," *Journal of Chemical Physics*, Vol. 139, No. 3, 2013, pp. 1–10.
doi:10.1063/1.4813070

[20] Bykova, N. G., and Kuznetsova, L. A., "Study of the Absorption Characteristics of Molecular Oxygen in the Schumann-Runge System at High Temperatures: I. Calculations of Absorption Spectra," *Optics and Spectroscopy*, Vol. 105, No. 5, 2008, pp. 668–673.
doi:10.1134/S0030400X08110040

[21] Andrienko, D. A., and Boyd, I. D., "High Fidelity Modeling of Thermal Relaxation and Dissociation of Oxygen," *Physics of Fluids*, Vol. 27, No. 11, 2015, pp. 1–25.

[22] Esposito, F., and Capitelli, M., "The Relaxation of Vibrationally Excited O_2 Molecules by Atomic Oxygen," *Chemical Physics Letters*, Vol. 443, No. 4, 2007, pp. 222–226.
doi:10.1016/j.cplett.2007.06.099

[23] Esposito, F., Capitelli, M., and Gorse, C., "Quasi-Classical Dynamics and Vibrational Kinetics of $N + N_2(v)$ System," *Chemical Physics*, Vol. 257, No. 2, 2000, pp. 193–202.
doi:10.1016/S0301-0104(00)00155-5

[24] Steele, D., Lippincott, E. R., and Vanderslice, J. T., "Comparative Study of Empirical Internuclear Potential Functions," *Reviews of Modern Physics*, Vol. 34, No. 2, 1962, p. 239–251.
doi:10.1103/RevModPhys.34.239

[25] Varandas, A., and Pais, A., "A Realistic Double Many-Body Expansion (DMBE) Potential Energy Surface for Ground-State O^3 from a Multiproperty Fit to ab initio Calculations, and to Experimental Spectroscopic, Inelastic Scattering, and Kinetic Isotope Thermal Rate Data," *Molecular Physics*, Vol. 65, No. 4, 1988, pp. 843–860.
doi:10.1080/00268978800101451

[26] Bortner, M., "A Review of Rate Constants of Selected Reactions of Interest in Re-Entry Flow Fields in the Atmosphere. Tech," National Bureau of Standards, U.S. Dept. of Commerce TR Note 484, 1969.

[27] Ibraguimova, L., Sergievskaya, A., and Shatalov, O., "Dissociation Rate Constants for Oxygen at Temperatures up to 11000 K," *Fluid Dynamics*, Vol. 48, No. 4, 2013, pp. 550–555.
doi:10.1134/S0015462813040145

[28] Park, C., "Hypersonic Aerothermodynamics," *International Journal of Aeronautical and Space Sciences*, Vol. 14, No. 1, 2013, pp. 1–10.
doi:10.5139/IJASS.2013.14.1.1

[29] Generalov, N., and Losev, S., "Vibrational Excitation and Decomposition of Molecular Oxygen and Carbon Dioxide Behind Shock Waves," *Journal of Quantum Spectroscopy and Radiative Transfer*, Vol. 6, No. 1, 1966, pp. 101–125.
doi:10.1016/0022-4073(66)90066-5